Self-Assembled Monolayers of Aromatic Selenolates on Noble Metal Substrates

A. Shaporenko,[†] P. Cyganik,[‡,§] M. Buck,[‡] A. Terfort,[||] and M. Zharnikov*[,†]

Angewandte Physikalische Chemie, Universität Heidelberg, Im Neuenheimer Feld 253, 69120 Heidelberg, Germany, School of Chemistry, St. Andrews University, North Haugh, St. Andrews KY16 9ST, United Kingdom, and Anorganische und Angewandte Chemie, Universität Hamburg, 20146 Hamburg, Germany

Received: February 10, 2005; In Final Form: April 7, 2005

Self-assembled monolayers (SAMs) formed from bis(biphenyl-4-yl) diselenide (BBPDSe) on Au(111) and Ag(111) substrates have been characterized by high-resolution X-ray photoelectron spectroscopy, near-edge X-ray absorption fine structure spectroscopy, infrared reflection absorption spectroscopy, water contact angle measurements, and scanning tunneling microscopy (STM). BBPDSe was found to form contamination-free, densely packed, and well-ordered biphenyl selenolate (BPSe) SAMs on both Au and Ag. Spectroscopic data suggest very similar packing density, orientational order, and molecular inclination in BPSe/Au and BPSe/Ag. STM data give a similar intermolecular spacing of 5.3 ± 0.4 Å on both Au and Ag but exhibit differences in the exact arrangement of the BPSe molecules on these two substrates, with the $(2\sqrt{3}\times\sqrt{3})$R30° and $(\sqrt{3}\times\sqrt{3})$R30° unit cells on Au and Ag, respectively. There is strong evidence for adsorbate-mediated substrate restructuring in the case of Au, whereas no clear statement on this issue can be made in the case of Ag. The film quality of the BPSe SAMs is superior to their thiol analogues, which is presumably related to a better ability of the selenolates to adjust the surface lattice of the substrate to the most favorable 2D arrangement of the adsorbate molecules. This suggests that aromatic selenolates represent an attractive alternative to the respective thiols.

1. Introduction

Tailoring surface properties such as wetting, adhesion, lubrication, corrosion, and biocompatibility is crucial for many frontier areas of modern science and technology. To a definite extent, this demand is met by self-assembled monolayers (SAMs), which are 2D polycrystalline films of semirigid molecules that are chemically anchored to a suitable substrate, giving it a new chemical identity.[1−5] A SAM-constituent combines three essential parts: a headgroup that binds strongly to the substrate; a tail group that constitutes the outer surface of the film; a spacer that separates head and tail groups. The performance of a SAM as a surfactant depends predominantly on the tail group but is also strongly influenced by its structure and packing density. The latter parameters, in their turn, result from the complex interplay of intermolecular and headgroup−substrate interactions, i.e., are essentially governed by the identity of the spacer and headgroup. Varying these building blocks, one can, in principle, design new SAMs for novel applications or improve the performance of already existing functional layers.

So far, the most popular headgroup for the preparation of SAMs on metal,[3,4,6] semiconductor (e.g. GaAs and InP),[7−9] and oxide (e.g. indium tin oxide)[10] substrates was thiolate, which provides a sufficiently strong and stable bonding to the respective surfaces. Both thiol and disulfide compounds were used as source materials since they provide the same bonding pattern in most cases due to the dissociation of the S−S bond upon the adsorption.[1,2] Focus systems were films of *n*-alkanethiols,[3,4] although recently thioaromatic SAMs became quite popular as well (see e.g. refs 6 and 11−25) in view of specific applications including conventional and chemical lithography[26−29] and molecular electronics.[12,30,31]

An alternative to thiols are selenols since the chemical properties of sulfur and selenium are rather similar. Both elements have the same electron configurations and are neighbors in the VI A column of the periodic table. Despite this similarity, there has been, however, relatively little work done to prepare, characterize, and use organic monolayers with selenolate headgroups. Only several compounds including alkaneselenols,[32,33] dialkyl diselenides,[34−36] benzeneselenol (BSe),[37−39] benzenediselenol,[40] and diphenyl diselenide (DPDSe)[37,39,41−43] were tested. Whereas it was shown that these compounds form SAMs on Au[32−34,37,41−43] and Ag[36,38] substrates in a way similar to that for thiols, the characterization was mostly performed by electrochemical methods and surface-enhanced Raman spectroscopy (SERS). Several controversial statements have been made. First, whereas Huang et al.[42] found that the Se−Se bond of DPDSe is cleaved to form benzeneselenolate upon adsorption on Au, Bandyopadhyay et al.[43] reported that this bond is preserved. Second, the results of Disner et al. suggested that DPDSe form multilayers on Au(111),[37] whereas the other authors claimed the formation of monolayer. Third, the selenium−gold bond was considered as both stronger[37,42,44] and weaker[32] than the sulfur−gold bond. An interesting finding is the difference in competitive adsorption of BSe and benzenethiol

* Corresponding author. E-mail: Michael.Zharnikov@urz.uni-heidelberg.de.
[†] Universität Heidelberg.
[‡] St. Andrews University.
[§] Present address: Physikalische Chemie I, Ruhr-Universitaet Bochum, Universitätsstr. 150, 44780 Bochum, Germany.
[||] Universität Hamburg.

10.1021/jp050731r CCC: $30.25
Published on Web 06/23/2005

(BT) on gold and silver substrates: whereas the adsorption of DPDSe is more favorable than that of diphenyl disulfide on gold,[42] the opposite situation occurs on Ag for BSe and BT.[38]

In this work we try to clarify some of the above-mentioned controversies and perform a detailed characterization of SAMs formed from bis(biphenyl) diselenide (BBPDSe: $C_6H_5C_6H_4Se-SeC_6H_4C_6H_5$) on gold and silver substrates by several complementary techniques. We intentionally took a biphenyl compound instead of previously studied BSe or DPDSe since the longer aromatic backbone is more favorable for the fabrication of high-quality SAMs,[21] which, subsequently, can serve as a basis for different practical applications.

In the following section we describe the experimental procedure and techniques. The results are presented and briefly discussed in section 3. An extended analysis of the data is given in section 4 followed by a summary in section 5.

2. Experimental Section

BBPDSe was synthesized according to the protocol given in ref 45. The gold and silver substrates were prepared by thermal evaporation of 200 nm of gold or 100 nm of silver (99.99% purity) onto mica or polished single-crystal silicon (100) wafers (Silicon Sense) primed with a 5 nm titanium adhesion layer. The mica substrates were preliminary annealed at 320 °C for 24 h prior to the metal evaporation, done at the same temperature. The evaporated films were polycrystalline, with a grain size of 20−50 nm for Si or a terrace size of 100−200 nm for mica as observed by atomic force microscopy and scanning tunneling microscopy. Both grains and terraces predominantly exhibit a (111) orientation.[46,47] The SAMs were formed by immersion of freshly prepared substrates into a 5 μmol BBPDSe solution in absolute ethanol at room temperature for 24 h. Due to a low solubility of BBPDSe in ethanol, the substance was preliminary solved in toluene to 1 mmol concentration. After immersion, the samples were carefully rinsed with pure ethanol, blown dry with argon, and kept, if necessary, for several days in argon-filled glass containers until the characterization. In addition, SAMs formed from biphenyl thiols (BPT: $C_6H_5C_6H_4SH$) were prepared by following the procedure described in ref 48 as a direct reference to the BPSe films. No evidence for impurities or oxidative degradation products was found in all the samples.

The samples were characterized by X-ray photoelectron spectroscopy (XPS), synchrotron-based high-resolution XPS (HRXPS), angle-resolved near-edge X-ray absorption fine structure (NEXAFS) spectroscopy, infrared reflection absorption spectroscopy (IRRAS), scanning tunneling microscopy (STM), and contact angle measurements. All experiments were performed at room temperature. The XPS, HRXPS, and NEXAFS measurements were carried out under UHV conditions at a base pressure better than 1.5×10^{-9} mbar. No noticeable damage by the primary X-rays occurred during the measurements.[29,49−51]

The HRXPS experiments were performed at the D1011 beamline of the MAX-lab synchrotron radiation facility in Lund, Sweden. Only the films on mica were used. The HRXPS spectra were collected in normal emission geometry at photon energies of 350 and 580 eV for the C 1s range, 150 eV for the Se 3d range, and 350 eV for the S 2p region. In addition, Au 4f and Ag 3d spectra were acquired and the O 1s range was monitored. The binding energy (BE) scale of every spectrum was individually calibrated using the Au $4f_{7/2}$ emission line of *n*-alkanethiol-covered Au substrate at 83.95 eV.[52] The energy resolution was better than 100 meV, which is noticeably smaller than the full widths at half-maximum (fwhm) of the photoemission peaks addressed in this study.

HRXPS spectra were fitted by symmetric Voigt functions and either a Shirley-type or linear background. To fit the Se $3d_{5/2,3/2}$ and S $2p_{3/2,1/2}$ doublets we used a pair of such peaks with the same fwhms, the branching ratios of 3:2 ($3d_{5/2}/3d_{3/2}$) and 2 ($2p_{3/2}/2p_{1/2}$) and spin−orbit splittings (verified by fit) of ≈0.86 eV ($3d_{5/2}/3d_{3/2}$) and ≈1.18 eV ($2p_{3/2}/2p_{1/2}$).[53] The accuracy of the resulting BE/fwhm values is 0.02−0.03 eV.

The NEXAFS measurements were performed at the HE-SGM beamline of the synchrotron storage ring BESSY II in Berlin, Germany. The spectra acquisition was carried out at the C K-edge in the partial electron yield mode with a retarding voltage of −150 V. Linear polarized synchrotron light with a polarization factor of ≈82% was used. The energy resolution was ≈0.40 eV. The incidence angle of the light was varied from 90° (**E**-vector in surface plane) to 20° (**E**-vector near surface normal) in steps of 10−20° to monitor the orientational order in the SAMs. The raw NEXAFS spectra were normalized to the incident photon flux by division through a spectrum of a clean, freshly sputtered gold sample. In the case of Ag substrate, a spectrum of clean silver was subtracted from the raw spectrum of a SAM sample before the normalization.[54,55] The energy scale was referenced to the pronounced π_1* resonance of highly oriented pyrolytic graphite at 285.38 eV.[56]

IRRAS measurements were performed with a dry-air-purged Bio-Rad FTIR spectrometer model FTS 175C equipped with a liquid nitrogen cooled MCT detector. All spectra were taken using *p*-polarized light incident at a fixed angle of 80° with respect to the surface normal. The spectra were measured at a resolution of 2 cm^{-1} and are reported in absorbance units $A = -\log R/R_0$, where R is the reflectivity of the substrate with the monolayer and R_0 is the reflectivity of the reference. Substrates covered with a SAM of perdeuterated hexadecanethiol were used as a reference.

STM measurements were carried out in air, using a PicoSPM (Molecular Imaging) microscope. Only the films on mica were used; the Au substrates were flame-annealed in a butane/oxygen flame before the SAM fabrication. The tips were prepared mechanically by cutting a 0.25 mm Pt/Ir alloy (8:2, Goodfellow) wire. The data were collected in constant-current mode using tunneling currents of 400 and 100 pA and sample biases of 0.4−0.5 and 0.2 V for the SAMs on the Au(111) and Ag(111) substrates, respectively. No tip-induced changes were observed.

Advancing and receding contact angles of Millipore water were measured on freshly prepared samples with a model G1 Krüss goniometer. The measurements were performed under ambient conditions with the needle tip in contact with the drop. At least three measurements at different locations on each sample were made. The averaged values are reported. The error was less than ±1°.

3. Results

3.1. XPS and HRXPS. Normalized Se 3d and C 1s HRXPS spectra of BPSe/Au and BPSe/Ag are presented in Figure 1, along with the corresponding fits (we will use the abbreviation BPSe for the films formed from BBPDSe). The results of the fitting and a quantitative analysis of these spectra are compiled in Table 1, along with the analogous data for the BPT/Au and BPT/Ag (see below). The Se 3d spectra of both BPSe/Au and BPSe/Ag exhibit a single Se $3d_{5/2,3/2}$ doublet, accompanied by a weak Au $5p_{3/2}$ emission. The BE position of this doublet (≈54.40 eV) is distinctly different from that for the bulk diselenides, e.g. didodecyl diselelenide (55.3 eV),[34] which

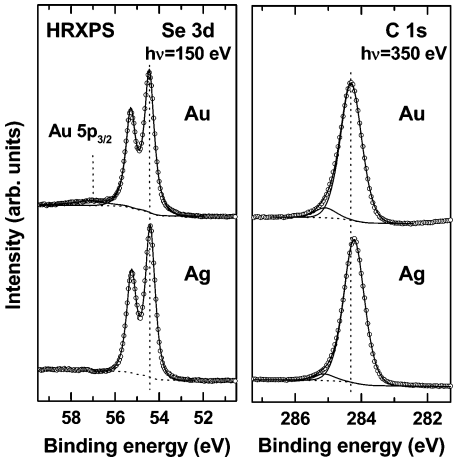

Figure 1. Normalized Se 3d and C 1s HRXPS spectra of BPSe/Au and BPSe/Ag (open circles) acquired at photon energies of 150 and 350 eV, respectively, along with the corresponding fits (solid lines). The positions of the Se $3d_{5/2}$ component and the C 1s main emission for BPSe/Au are marked by the dotted lines. A background is shown.

TABLE 1: Binding Energy Positions (eV) and Fwhm's (eV; in Parentheses) of the Photoemission Peaks for BPSe and BPT Films on Au and Ag

film	C 1s main	C 1s additional	Se $3d_{5/2}$ or S $2p_{3/2}$
BPSe/Au	284.31 (0.76)	285.09 (0.76)	54.44 (0.53)
BPSe/Ag	284.22 (0.75)	285.12 (0.75)	54.40 (0.53)
BPT/Au	284.17 (0.80)	284.68 (0.80)	162.03 (0.66)
BPT/Ag	284.38 (0.78)	284.93 (0.78)	162.08 (0.56)

suggests the cleavage of the covalent Se−Se bond and building of a selenolate−metal bond upon the adsorption of BBPDSe on Au and Ag. Note that there is a similar difference between the BE positions of the S 2p doublet in thiolate SAMs on noble metal substrates and those in nonbound thiol and dithiol compounds.[47,57]

The formation of the selenolate−metal bond can also be monitored using a substrate emission, e.g., Au $4f_{7/2}$ in the case of Au. The Au $4f_{7/2}$ HRXPS spectra of clean gold and BPSe/Au are presented in Figure 2. The former spectrum exhibits a splitting of the Au $4f_{7/2}$ emission in two components at ≈83.95 and ≈83.65 eV, which can be assigned to the gold atoms in the bulk and topmost surface layer, respectively.[47] This assignment is supported by the intensity decrease of the surface component with increasing kinetic energy of the photoelectrons[36] and by the good agreement of the observed surface core level shift of −0.31 eV with literature values.[47,58−60] Upon the adsorption of BBPDSe, the surface component shifts to higher binding energy, merging with the bulk one. The fwhm of the joint peak is then directly dependent on the BE spacing between both components. Since the fwhm of these components is known (from the spectrum of the clean Au) and constant at a given PE, the fwhm of the joint Au $4f_{7/2}$ emission represents a suitable fingerprint to describe the BE spacing between surface and bulk components, which can be directly used to evaluate the adsorbate-induced shift of the surface component. The fwhm values for clean Au, BPSe/Au, and BPT/Au, where a similar shift of the Au $4f_{7/2}$ surface component was observed,[47] are compiled in Table 2. The data for two different photon energies are presented; the higher fwhm value for the higher photon energy is related to increasing energy spreading of the primary photon beam. As seen in Table 2, the Au $4f_{7/2}$ fwhms for BPSe/Au and BPT/Au are very close to each other, which suggest similar extents of the charge transfer from the substrate to both selenolate and thiolate headgroups attached to the biphenyl

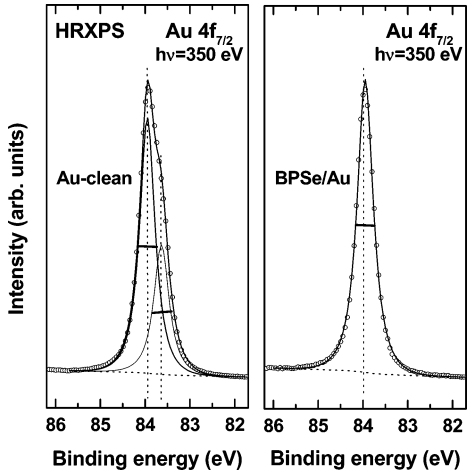

Figure 2. Normalized Au $4f_{7/2}$ HRXPS spectra of clean Au and BPSe/Au acquired at a photon energy of 350 eV. The decomposition of the former spectrum into the bulk and surface components is shown.

TABLE 2: Fwhm (eV) of the Bulk and Surface Au $4f_{7/2}$ Components for Clean Au, and Fwhm (eV) of the Joint Au $4f_{7/2}$ Emission for BPSe/Au and BPT/Au[a]

	photon energy	
system	350 eV	580 eV
clean Au	0.405	0.424
BPSe/Au	0.427	0.440
BPT/Au	0.424	0.443

[a] The data for two different photon energies are presented; the higher fwhm value for the higher photon energy is related to increasing energy spreading of the primary X-ray beam.

spacer. The adsorbate-induced shift of the Au $4f_{7/2}$ surface component can be estimated at 0.28 eV. Note that for the Ag substrate a similar analysis is difficult, since the surface core level shift for the clean Ag (111) surface is quite small, so that the bulk and surface components are merged together.[47]

Also in the case of the Se 3d doublet, fwhm of the Se $3d_{5/2}$ and Se $3d_{3/2}$ components is an important parameter. Since the instrumental spreading was almost negligible, the value of fwhm is characteristic of the inhomogeneity of the bonding configurations (e.g. the distribution of the absorption sites) for the selenolate headgroups. Small Se $3d_{5/2,3/2}$ fwhms for both BPSe/Au and BPSe/Ag suggest that the arrangement of the selenolate headgroups on both substrates is close to a commensurate one (for some other Se-derived SAMs, noticeably larger values of the Se $3d_{5/2,3/2}$ fwhm were observed).[36] This is distinctly different from the BPT case, where a comparably large fwhm is observed on both Au and Ag, with a larger value for Au (see Table 1), assuming a superposition of several different adsorption sites for the thiolate headgroups.[47,61]

The C 1s HRXPS spectra of BPSe/Au and BPSe/Ag in Figure 1 exhibit a main emission assigned to the biphenyl backbone and a weak high binding energy shoulder, which can be alternatively ascribed to the carbon atom bonded to Se or a shake up excitation in the aromatic matrix.[47,61] The presence of the shoulder can be deduced from a weak asymmetry of the C 1s peak. The positions of the main emission in the BPSe SAMs are close to those in the BPT films (Table 1). The C1s fwhms are quite similar as well, with even smaller values for the BPSe layers, which can be considered as an indirect manifestation of their higher quality.

In addition, the intensity of the C 1s emission was evaluated and the effective thickness of the BPSe SAMs was determined from the I_{C1s}/I_{Au4f} and I_{C1s}/I_{Ag3d} intensity ratios, using the

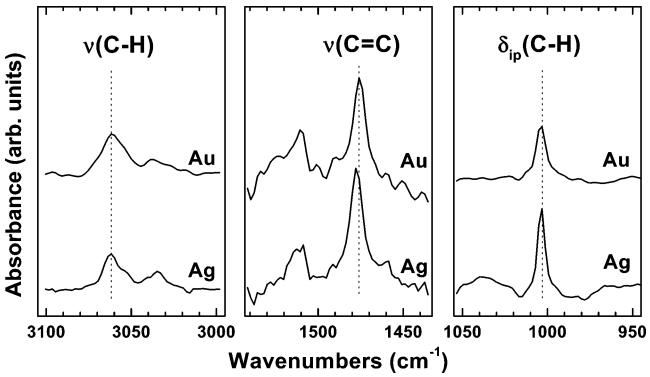

Figure 3. IRRAS spectra of BPSe/Au and BPSe/Ag for three characteristic spectral ranges. The characteristic absorption bands are marked.

attenuation lengths reported in ref 62 (the procedure has been verified for several reference samples). The derived values are 11.9 and 12.0 Å for BPSe/Au and BPSe/Ag, respectively. The similarity of these values suggests similar packing densities in BPSe/Au and BPSe/Ag. Also, these values correlate with the previous estimates of 12.4 Å for BPT/Au[12] and 13 ± 1 Å for differently substituted X-BPT/Au and X-BPT/Ag,[23,48] considering the part of the substitution. The comparison of the thickness data for the BPSe and BPT SAMs implies a weaker effect by the substrate on the packing density in the former systems.

3.2. IRRAS. The IRRAS spectra of the BPSe films for three selected regions are presented in Figure 3. These spectra exhibit characteristic absorption bands of the biphenyl moiety, namely the C−H stretching vibration at ≈3062 cm^{-1}, the C═C stretching mode at ≈1475 cm^{-1}, and the C−H bending mode at ≈1004 cm^{-1} (the mode assignment was performed in accordance with refs 63−65). The transition dipole moments (TDM) of the C═C stretching and C−H bending modes are oriented along the 4−4′ axis of the biphenyl moieties—these modes are most intense features in the adsorption spectra. The TDM of the C−H stretching mode is perpendicular to the 4−4′-axis and parallel to the ring plane; the intensity of this mode is, however, quite weak. Important is the disappearance of the C−H deformation band at 807 cm^{-1} (the respective spectral range is not shown), which is rather intense in the IR spectra of the biphenyl- and terphenyl-based bulk materials.[24,65,66] Thus, the modes with the TDM parallel to the 4−4′ axis are rather intense in the IR spectra of BPSe/Au and BPSe/Ag, whereas the modes with the TDM perpendicular to this axis are either weak or not observed at all. Considering the selection rules for IR spectroscopy on surfaces (only those vibrations are seen which have a component of the TDM perpendicular to the substrate plane), we can definitely conclude that the biphenyl moieties in the BPSe films have an upright orientation both on Au and Ag.

3.3. NEXAFS. Carbon K-edge NEXAFS spectra of BPSe/Au and BPSe/Ag acquired at three selected X-ray incidence angles are presented in Figures 4 and 5, respectively, along with the difference between the "90°" and "20°" spectra (bottom curves). The spectra exhibit characteristic absorption resonances of the phenyl rings[21,24,25,67−69] and are dominated by the intense π_1* resonance at ≈285.0 eV, which is accompanied by the weaker π_2* resonance at ≈288.9 eV, a R* resonance at ≈287.5 eV, and several broad σ* resonances at higher photon energies.

The NEXAFS spectra of BPSe/Au and BPSe/Ag exhibit a pronounced linear dichroism, i.e., a dependence of the absorption resonance intensity on the X-rays incidence angle. Such a dependence is a fingerprint of the orientational order and is related to the fact that the cross section of the resonant photoexcitation process depends on the orientation of the electric field vector of the synchrotron light with respect to the molecular orbital of interest.[68] Using the entire sets of spectra acquired at different incidence angles, average tilt angles of the biphenyl backbones in the BPSe films were estimated. For this purpose, the intensity of absorption resonances I was monitored as a function of the X-ray incidence angle θ and the resulting

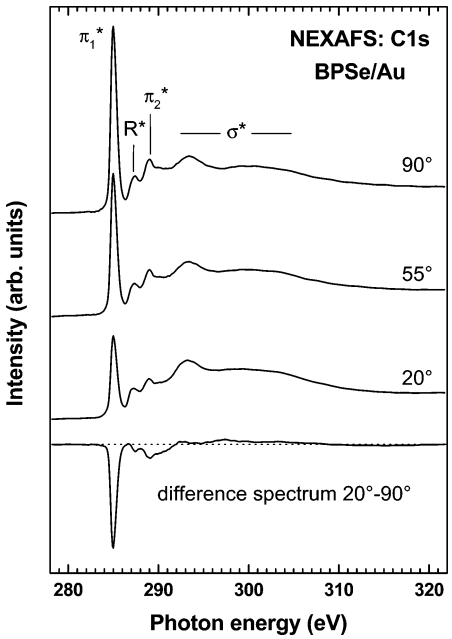

Figure 4. Carbon K-edge NEXAFS spectra of BPSe/Au acquired at X-ray incident angles of 90, 55, and 20°, respectively, along with the difference between the 90 and 20° spectra. The dotted line corresponds to zero. The characteristic absorption resonances are marked.

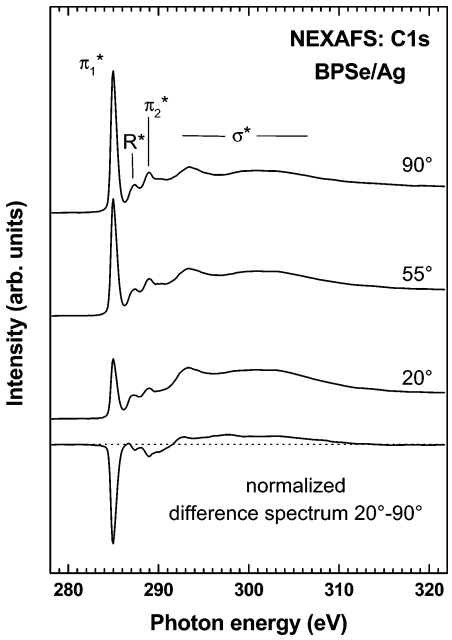

Figure 5. Carbon K-edge NEXAFS spectra of BPSe/Ag acquired at X-ray incident angles of 90, 55, and 20°, respectively, along with the difference between the 90 and 20° spectra. The difference spectrum is normalized to the π_1* intensity ratio between the 55° spectra of BPSe/Ag and BPSe/Au, for direct comparison to the respective spectrum of BPSe/Au. The dotted line corresponds to zero. The characteristic absorption resonances are marked.

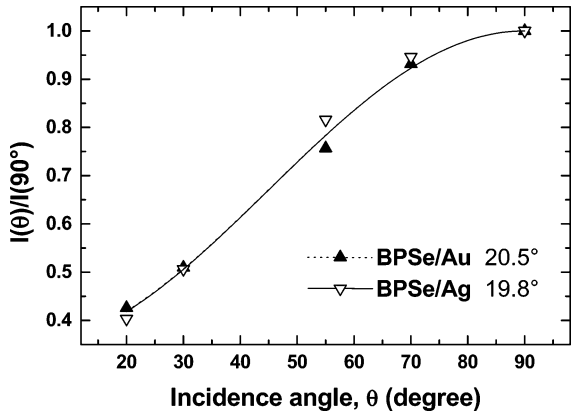

Figure 6. Angular dependence of the π_1* resonance intensity ratio $I(\theta)/I(90°)$ for BPSe/Au (up triangles) and BPSe/Ag (down triangles), along with the best theoretical fits according to eq 1 (dotted and solid lines, respectively). The fits for BPSe/Au and BPSe/Ag overlap.

dependence evaluated according to the theoretical expression (for a vector-type orbital)[68]

$$I(\alpha,\theta) = A\left\{P \times \frac{1}{3}\left[1 + \frac{1}{2}\cdot(3\cos^2\theta - 1)(3\cos^2\alpha - 1)\right] + (1-P)(1/2)\sin^2\alpha\right\} \quad (1)$$

where A is a constant, P is a polarization factor of the X-rays, and α is the average tilt angle of the molecular orbital.

For the evaluation, the most intense π_1* resonance has been selected; its TDM is oriented perpendicular to the ring plane. The expression (1) was slightly modified to include the twist of the biphenyl backbones.[8,70] A herringbone packing of these backbones with a twist angle of 32°, which is close to that for bulk aromatic compounds, was assumed.[13,17,71,72] Note that a herringbone structure of the aromatic moieties optimizes the intermolecular interaction in the densely packed 2D-layers and is, in particular, typical for aromatic thiol-derived SAMs on Au.[17,72,73] To avoid normalization problems, not the absolute intensities but the intensity ratios $I(\theta)/I(90°)$ were analyzed,[68] where $I(\theta)$ and $I(90°)$ are the intensities of the π_1* resonance at X-ray incidence angles of θ and 90°. The respective angular dependences of $I(\theta)/I(90°)$ are presented in Figure 6, along with the best theoretical fits according to eq 1: the curves for Au and Ag are very close to each other. The derived values of the average tilt angles of the biphenyl backbones in BPSe/Au and BPSe/Ag are 20.5° and 19.8°, respectively; the accuracy of these values is ±3−5°, which is just a general accuracy of the NEXAFS experiment and data evaluation. For comparison, the analogous parameters of the BPT/Au and BPT/Ag are 23 and 18°, respectively; these values were derived within the same assumptions as in this study.[21]

The molecular inclination is very similar in BPSe/Au and BPSe/Ag, which agrees with the conclusions derived on the basis of the XPS and HRXPS data. The effect of the substrate is, thus, almost negligible, within the accuracy of the experiments, which is in contrast to the BPT case. Note, however, that the average tilt angle is representative of both molecular inclination and orientational order, so that a higher value of this parameter for BPT/Au as compared to all other systems under consideration might partly reflect a poorer structural quality (crystallinity) of this particular film.

3.4. STM. STM data for the BPSe/Au are summarized in Figure 7. Comparison with the analogous images of clean Au substrate (not shown) showed that the formation of the BPSe films causes pronounced changes in the substrate morphology, i.e., creation of small islands and changes in the preferred orientation of the step edges (see Figure 7a). Whereas triangular facets with ⟨110⟩ step edges are typical for the clean Au(111) substrate,[74] ⟨211⟩ step edges were found after the adsorption of the BPSe molecules (Figure 7a). Note that such an effect was not observed for a very similar thiol-derived system, 4-methyl-4′-mercaptobiphenyl, $CH_3C_6H_4C_6H_4SH$ (MBPT) on Au(111),[72] but was seen for some biphenyl-substituted alkanethiols.[75] Also, such an extended reorientation of step edges was not recorded for BSe, where only SAM-induced stabilization of the hexagonal facets occurred.[37] Thus, this effect cannot be exclusively related to the selenide headgroup or to the biphenyl moiety but is the result of a complex interplay of different interactions in the SAM−substrate system.

Another obvious feature seen in Figure 7a is the presence of dark lines which run parallel to the "new" step edges, i.e., along the ⟨211⟩ directions, and have a depth of ≈2.0−2.2 Å (see cross section in Figure 7c). Both orientation and depth of these lines are strikingly similar to those observed in a recent study of alkaneselenolates on Au, which assigned the depression to rows of missing substrate atoms.[35] Since the molecules in the two studies are rather different but the depth value is identical, we believe in the common origin of the depression lines. The somewhat smaller height difference compared to the step height on Au(111) (2.4 Å) is believed to be due to an electronic effect, since bonding and electronic structure in these narrow depressions are likely to be different from extended terraces. A tip size effect can be excluded since, despite the narrow width of the depressions, the molecular structure is partially resolved inside, as shown in the high-resolution STM images (Figure 7c,d). Note that, unlike for the alkaneselenolates[35] where the depressions were only observed in regions of less dense packing, the BPSe SAMs show this feature at dense packing, which, in further contrast to the alkaneselenolate system, was the only structure observed. A further observation is that the depressions are located at domain boundaries (Figure 7c). Common orientation of these boundaries and the "new" step edges proves strong correlation between changes in the substrate atom arrangement and formation of the film structure. Note that a correlation of substrate depressions with the locations of domain boundaries has also been observed in the case of thiol-based SAMs,[76−80] which, however, lack the pronounced anisotropy of BPSe/Au.

The details of the molecular structure of BPSe/Au are visible in the high-resolution STM image in Figure 7d, while a schematic, simplified representation of this structure is given in Figure 7e. The dimensions of the 2D unit cell, shown in Figure 7d,e, were determined from the height profiles along the molecular rows (e.g. along the lines A and B in Figure 7d) and amount to $a = 5.3 \pm 0.4$ Å and $b = 10.3 \pm 0.7$ Å. This unit cell closely corresponds to a $(2\sqrt{3}\times\sqrt{3})$R30° structure with two molecules/unit cell, as shown in Figure 7e.

Whereas high-quality molecular-resolution images were acquired for BPSe/Au, STM did, for presently unknown reasons, not work equally well in the case of BPSe/Ag even though molecular resolution was also achieved. Some STM data for the latter film are presented in Figure 8. Similarly to Au(111), the adsorbate-induced formation of substrate islands was observed in large scale STM images of BPSe/Ag (Figure 8a), even though the island size (5−40 nm) was significantly smaller than that for BPSe/Au. The high-resolution images of BPSe/Ag (Figure 8b) exhibited a molecular layer, which reveals a hexagonal-like arrangement on a short-range length scale but a less ordered structure on a long-range one. The preferred

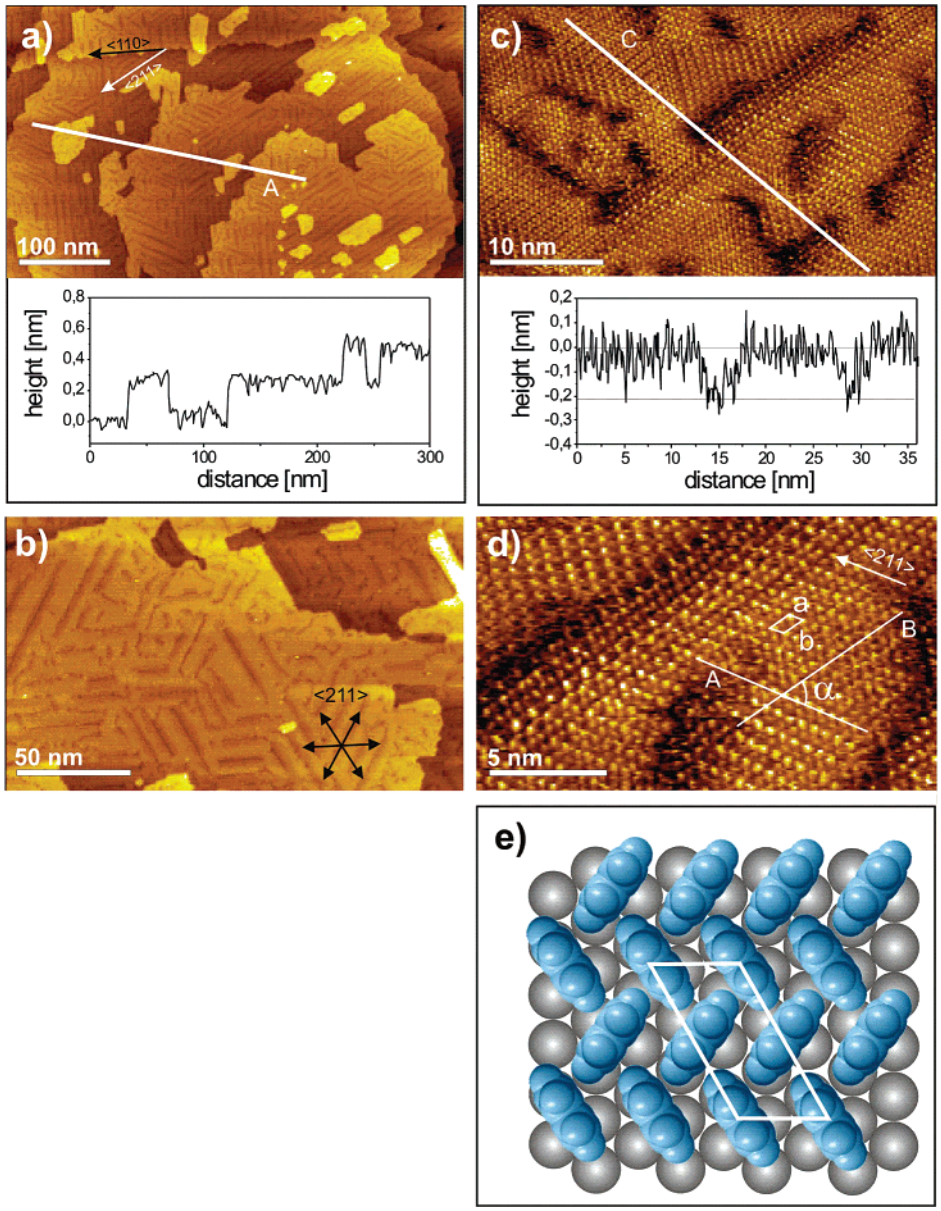

Figure 7. STM images of BPSe/Au taken at different resolutions (a−d). In the lower part of images a and c height profiles along the lines A and C, respectively, are shown. The oblique box depicted in (d) marks the $(2\sqrt{3}\times\sqrt{3})$R30° oblique unit cell. Its average size ($a = 5.3 \pm 0.4$ Å, $b = 10.3 \pm 0.7$ Å, and $\alpha = 58 \pm 2°$) was calculated from the cross-sectional height profiles taken along the directions marked by the lines A and B for a set of 5 different images.

hexagonal-like arrangement is highlighted by a Fourier transformation of this image, which is presented in Figure 8c—it shows a hexagonal pattern, even though with a slight asymmetry. To estimate the average intermolecular distance, radial averaging of this transformation was performed, as shown in Figure 8d. There a small peak 0.187 $Å^{-1}$ (marked by the arrow) in the obtained radial distribution, which corresponds to the average intermolecular distance of ≈5.3 ± 0.4 Å. This value is significantly smaller than a distance of 7.6 Å in hexagonal $(\sqrt{7}\times\sqrt{7})$R19.1° structure observed for a Se adlayer on Ag(111),[81] underlining, thus, the role of the aromatic backbone in BPSe/Ag. Also, this value suggests a close-to-commensurate lattice on short-range length scale in the latter film, along with the packing density comparable to BPSe/Au. It is not clear at present whether the $(\sqrt{3}\times\sqrt{3})$R30° unit cell in BPSe/Ag compared to $(2\sqrt{3}\times\sqrt{3})$R30° in BPSe/Au is real or whether it is a matter of the imaging conditions and/or the somewhat lower quality of the STM data.

3.5. Wetting Properties. The advancing (θ_a) and receding (θ_r) water contact angles for BPSe/Au and BPSe/Ag are given in Table 3, along with the analogous data for the BPT films.[23] Both θ_a and θ_r for the BPSe SAMs are noticeably higher than the respective values for the BPT films, which suggest a better quality of the former SAMs. The contact angles for BPSe/Au and BPSe/Ag are even approaching the analogous values for the most densely packed thiol-derived aromatic SAMs—terphenyl-substituted alkanethiols (78−80 and 89−93° for θ_a and θ_r, respectively).[82] The larger values of the contact angle hysteresis ($\Delta\theta = \theta_a - \theta_r$) in the BPSe films than in the BPT SAMs are presumably related to a reduced surface roughness of the specially annealed Au substrates used in ref 23. It is well-known that the substrate roughness has a direct impact on the hysteresis value.[23] A contact angle hysteresis of about 20° is typical for aromatic SAMs, if no special care is taken to reduce the roughness of the substrate.[23]

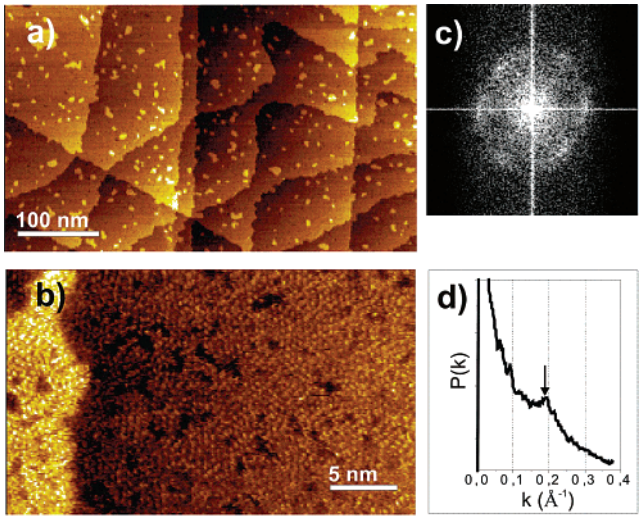

Figure 8. STM images of BPSe/Ag taken at different resolutions (a−b). A 2D Fourier transformation of the data presented in (b) and a power spectrum $P(k)$ obtained after radial averaging of this transformation are shown in (c) and (d), respectively. The arrow in (d) marks the position of the cusp at 0.187 $Å^{-1}$, which corresponds to the average distance of about 5.3 Å. Tunneling parameters are $U = 0.2$ V and $I =$ 100 pA.

TABLE 3: Advancing (θ_a, deg) and Receding (θ_r, deg) Water Contact Angles for the BPSe and BPT Films on Au and Ag

	Au		Ag	
film	θ_{adv}	θ_{rec}	θ_{adv}	θ_{rec}
BPSe	86	76	88	77
BPT[23]	73	69	71	66

Comparing the contact angle values for the BPSe SAMs on Au and Ag, we can conclude that the wetting properties of these two films are very similar. This is an additional evidence, underlining the similarity in the structure and parameters of BPSe/Au and BPSe/Ag.

4. Discussion

All experimental data imply that BBPDSe form contamination-free, densely packed, and well-ordered BPSe SAMs on Au(111) and Ag(111). The molecules are bound to the substrate via a selenolate−metal linkage, while the biphenyl backbones have an upright orientation with an average tilt angle of about 20°. The selenolate−metal linkage is formed upon the adsorption of the BBPDSe molecules, via cleavage of the Se−Se bond, similar to the formation of the thiolate bonds from the disulfide precursors. The scission of diselenide and disulfide bonds occurs in a similar way—by an oxidative addition mechanism. The observed adsorption-induced scission of the Se−Se bond in deselenides agrees with most of the previous results obtained for DPDSe/Au by SERS.[39,42]

All experimental data suggest similar packing densities, orientational order, and molecular inclinations in BPSe/Au and BPSe/Ag. This is in pronounced contrast to the behavior of thiol-derived aromatic SAMs and, in particular, to the BPT films on these two substrates, where a higher packing density and a smaller molecular inclination are observed on Ag compared to Au.[21] Considering that the only difference between the BPT and BPSe molecules is the headgroup, different bond strengths and/or even different bonding configurations for the selenolate and thiolate headgroups can be assumed. This agrees with previous results on BSe and BT SAMs, for which most studies claim a stronger bonding of the BSe molecules on Au[37,42,44] and a weaker bonding on Ag[38] as compared to the BT species. As to the bonding configuration of the selenolate headgroup, no data on this issue have been reported so far for aromatic SAMs. At the same time, in aliphatic SAMs, the selenolate headgroup is assumed to have the same sp^3 bonding configuration on Au and Ag,[36] which is in contrast to sp^3 and sp configurations suggested for thiolate headgroups on Au and Ag, respectively.[65,82,83]

Apart from the substrate effect, the overall quality of the BPSe SAMs is remarkably higher than that of BPT or very similar MBPT films, at least on Au (there is no literature data for Ag). For MBPT/Au, a poor film quality was reported[20] and a rather poor film crystallinity was observed.[84] In contrast, BPSe forms SAMs of excellent crystallinity on Au.

According to the STM data, there is no differences in the intermolecular spacing of the BPSe moieties (5.3 ± 0.4 Å) on Au and Ag within the experimental error. This substrate independent packing of the molecules agrees very well with all other experimental data. However, the high-quality molecular resolution images reveal some differences between BPSe/Au and BPSe/Ag. For the latter, the overall quality is significantly lower and the number of molecules/unit cell is one compared to two for Au. The reason for this is not clear at present, since it can be explained by differences in either the real structure or in the STM imaging process. We tend to believe in the latter, given the fact that the spectroscopic results do not suggest substantial differences. This view is consistent with the literature data, which suggest that imaging of SAMs on Ag is much more difficult than on Au. There are only few publications presenting high-quality molecular-resolution STM images for aliphatic thiol-derived SAMs on Ag(111)[85,86] and none for aromatic thiol-derived SAMs on Ag(111).

While the STM data for BPSe/Au are generally compatible with a commensurate molecular lattice on Au(111), the strikingly anisotropic contrast due to domain boundaries running along the ⟨211⟩ directions indicates a significant amount of anisotropic stress, which is relieved through domain formation and restructuring of the Se/Au interface. Both the packing of the biphenyl units and the influence of the selenium are considered to contribute. There is a significantly stronger influence of selenium on gold compared to sulfur, which is, in particular, seen from the comparison of alkanethiols with alkaneselenols. As mentioned above, contrast features due to missing rows of Au atoms, similar to BPSe SAMs, were seen for the latter systems,[35] whereas this was not the case for alkanethiols. In its turn, the contribution of the biphenyl units stems from mismatch of their optimal packing and the underlying (111) lattice of the gold substrate; in particular, the preferred packing of bulk biphenyl deviates slightly from a hexagonal arrangement.[87] Under these circumstances, the restructuring can be mediated by the "wish" of the selenolate groups to keep their preferred adsorption site on Au(111), which is only possible if the topmost Au layer reconstructs, adapting to the optimal packing of the BPSe molecules. Within every reconstruction domain, these molecules form an almost commensurate structure on the reconstructed surface. The "almost" reflects the fact that there can be a growing (even though slight) deviation from the optimal adsorption site going from the domain centers to their boundaries, which can be an additional reason for the domain formation and restructuring of the Se/Au interface, since the stress is accumulating. This means that the observed structure of the BPSe SAMs is not exactly commensurate and, therefore, the $(2\sqrt{3}\times\sqrt{3})R30°$ is an approximation, only.

In contrast to Au, no extended surface reconstruction and pronounced anisotropy of the domain boundaries were observed for BPSe/Ag. The reason for this difference is not clear at present, but differences in the corrugation of the molecule−substrate potential could account for it. However, the quality of the STM images for BPSe/Ag is inferior to those for BPSe/Au, so that it is also possible that fine details of the molecular arrangements in the former system can just not be properly seen.

5. Conclusions

Several complementary experimental techniques were applied to characterize SAMs formed from BBPDSe on Au(111) and Ag(111). The results suggest the formation of contamination-free, densely packed, and well-ordered BPSe SAMs on these substrates. The molecules are bound to the substrate via a selenolate−metal linkage, which is formed after the cleavage of the Se−Se bond in the BBPDSe molecules, mediated by the metal substrate. The biphenyl backbones were found to have an upright orientation with an average tilt angle of about 20°.

Spectroscopic data show unanimously that BPSe/Au and BPSe/Ag are very similar, including similar packing density, orientational order, molecular inclination, and wetting properties. This is in striking contrast to the behavior of thiol-derived aromatic SAMs, where a higher packing density and a smaller molecular inclination are observed on Ag. This underlines the role of the selenolate headgroup.

Molecular resolution STM images were acquired, and in full agreement with the spectroscopic data, no significant influence of the substrate on the intermolecular spacing (5.3 ± 0.4 Å) was identified. At the same time, the unit cells of the BPSe molecules on Au and Ag, approximated with the $(2\sqrt{3}\times\sqrt{3})$R30° and $(\sqrt{3}\times\sqrt{3})$R30° arrangements, appear slightly different. In addition, a pronounced anisotropy of the domains and depressions in the substrate at the domain boundaries were observed on Au, suggesting an adsorbate-mediated restructuring of the Au(111) surface. We assume that the arrangement of the BPSe molecules within every domain deviates weekly from the commensurate $(2\sqrt{3}\times\sqrt{3})$R30° structure, resulting in an increasing deviation from an optimal adsorption site going from the center of a domain to its boundaries.

An important result of the study presented here is that the structural quality of the BPSe SAMs is much better than that of their thiol analogues, which is presumably related to a better ability of the selenolates to adjust the surface lattice of the substrate to the most favorable 2D arrangement of the adsorbate molecules. While for thiols an alkane spacer seems to be required to yield good quality layers,[73] this appears not to be the case for selenolates. This might be of significant interest for molecular electronics, since a pure aromatic backbone has a better conductivity than a hybrid, aromatic−aliphatic one.[88,89] In addition, the contact transmission of the selenolate headgroup is superior to the thiolate,[90,91] which is a further argument in favor of selenolate-based systems.

Acknowledgment. We thank M. Grunze for the support of this work, A. Küller for providing us with the BPT substance, Ch. Wöll (Universität Bochum) for providing us with the equipment for the NEXAFS measurements, L. S. O. Johansson (Karlstad University) for the cooperation at MAX-lab, and the BESSY II and MAX-lab staff for the assistance during the experiments at the synchrotrons. This work was supported by the German BMBF (Grant 05KS4VHA/4), European Community (Access to Research Infrastructure action of the Improving Human Potential Program), the Scottish Higher Education Funding Council, and The Leverhulme Trust.

References and Notes

(1) Ulman, A. *An Introduction to Ultrathin Organic Films: Langmuir-Blodgett to Self-Assembly*; Academic Press: New York, 1991.
(2) Ulman, A. *Chem. Rev.* **1996**, *96*, 1533.
(3) *Thin films: self-assembled monolayers of thiols*; Ulman A., Ed.; Academic Press: San Diego, CA, 1998.
(4) Schreiber, F. *Prog. Surf. Sci.* **2000**, *65*, 151.
(5) Schreiber, F. *J. Phys.: Condens. Matter.* **2004**, *16*, R881.
(6) Ulman, A. *Acc. Chem. Res.* **2001**, *34*, 855.
(7) Sheen, C. W.; Shi, J.-X.; Martensson, J.; Parikh, A. N.; Allara, D. L. *J. Am. Chem. Soc.* **1992**, *114*, 1514.
(8) Shaporenko, A.; Adlkofer, K.; Johansson, L. S. O.; Tanaka, M.; Zharnikov, M. *Langmuir* **2003**, *19*, 4992.
(9) Zerulla, D.; Chasse, T. *Langmuir* **2002**, *18*, 5392.
(10) Yan, C.; Zharnikov, M.; Gölzhäuser, A.; Grunze, M. *Langmuir* **2000**, *16*, 6208.
(11) Sabatani, E.; Cohen-Boulakia, J.; Bruening, M; Rubinstein, I. *Langmuir* **1993**, *9*, 2974.
(12) Tour, J. M.; Jones, L., II; Pearson, D. L.; Lamba, J. S.; Burgin, T. P.; Whitesides, G. M.; Allara, D. L.; Parikh, A. N.; Atre, S. V. *J. Am. Chem. Soc.* **1995**, *117*, 9529.
(13) Dhirani, A.-A.; Zehner, W.; Hsung, R. P.; Guyot-Sionnest, P.; Sita, L. *J. Am. Chem. Soc.* **1996**, *118*, 3319.
(14) Tao, Y.-T.; Wu, C.-C.; Eu, J.-Y.; Lin, W.-L. *Langmuir* **1997**, *13*, 4018.
(15) Kang, J. F.; Jordan, R.; Ulman, A. *Langmuir* **1998**, *14*, 3983.
(16) Kang, J. F.; Liao, S.; Jordan, R.; Ulman, A. *J. Am. Chem. Soc.* **1998**, *120*, 9662.
(17) Himmel, H.-J.; Terfort, A.; Wöll, Ch. *J. Am. Chem. Soc.* **1998**, *120*, 12069.
(18) Kang, J. F.; Ulman, A.; Liao, S.; Jordan, R. *Langmuir* **1999**, *15*, 2095.
(19) Ishida, T.; Choi, N.; Mizutani, W.; Tokumoto, H.; Kojima, I.; Azehara, H.; Hokari, H.; Akiba, U.; Fujihira, M. *Langmuir* **1999**, *15*, 6799.
(20) Leung, T. Y. B.; Schwartz, P.; Scoles, G.; Schreiber, F.; Ulman, A. *Surf. Sci.* **2000**, *458*, 34.
(21) Frey, S.; Stadler, V.; Heister, K.; Zharnikov, M.; Grunze, M.; Zeysing, B.; Terfort, A. *Langmuir* **2001**, *17*, 2408.
(22) Ishida, T.; Mizutani, W.; Azehara, H.; Sato, F.; Choi, N.; Akiba, U.; Fujihira, M.; Tokumoto, H. *Langmuir* **2001**, *17*, 7459.
(23) Kang, J. F.; Ulman, A.; Liao, S.; Jordan, R.; Yang, G.; Liu, G.-y. *Langmuir* **2001**, *17*, 95.
(24) Fuxen, C.; Azzam, W.; Arnold, R.; Witte, G.; Terfort, A.; Wöll, Ch. *Langmuir* **2001**, *17*, 3689.
(25) Zharnikov, M.; Grunze, M. *J. Phys.: Condens. Matter.* **2001**, *13*, 11333.
(26) Geyer, W.; Stadler, V.; Eck, W.; Zharnikov, M.; Gölzhäuser, A.; Grunze, M. *Appl. Phys. Lett.* **1999**, *75*, 2401.
(27) Eck, W.; Stadler, V.; Geyer, W.; Zharnikov, M.; Gölzhäuser, A.; Grunze, M. *Adv. Mater.* **2000**, *12*, 805.
(28) Gölzhäuser, A.; Eck, W.; Geyer, W.; Stadler, V.; Weimann, T.; Hinze, P.; Grunze, M. *Adv. Mater.* **2001**, *13*, 806.
(29) Zharnikov, M.; Grunze, M. *J. Vac. Sci. Technol., B* **2002**, *20*, 1793.
(30) Bumm, L. A.; Arnold, J. J.; Cygan, M. T.; Dunbar, T. D.; Burgin, T. P.; Jones, L., II; Allara, D. L.; Tour, J. M.; Weiss, P. S. *Science* **1996**, *271*, 1705.
(31) Adams, D. M.; Brus, L.; Chidsey, C. E. D.; Creager, S.; Creutz, C.; Kagan, C. R.; Kamat, P. V.; Lieberman, M.; Lindsay, S.; Marcus, R. A.; Metzger, R. M.; Michel-Beyerle, M. E.; Miller, J. R.; Newton, M. D.; Rolison, D. R.; Sankey, O.; Schanze, K. S.; Yardley, J.; Zhu, X. *J. Phys. Chem. B* **2003**, *107*, 6668.
(32) Samant, M. G.; Brown, C. A.; Gordon, J. G., II. *Langmuir* **1992**, *8*, 1615.
(33) Nakano, K.; Sato, T.; Tazaki, M.; Takagi, M. *Langmuir* **2000**, *16*, 2225.
(34) Yee, C. K.; Ulman, A.; Ruiz, J. D.; Parikh, A.; White, H.; Rafailovich, M. *Langmuir* **2003**, *19*, 9450.
(35) Monnell, J. D.; Stapleton, J. J.; Jackiw, J. J.; Dunbar, T.; Reinerth, W. A.; Dirk, S. M.; Tour, J. M.; Allara, D. L.; Weiss, P. S. *J. Phys. Chem. B* **2004**, *108*, 9834.
(36) Shaporenko, A.; Ulman, A.; Terfort, A.; Zharnikov M. *J. Phys. Chem. B* **2005**, *109*, 3898.
(37) Dishner, M. H.; Hemminger, J. C.; Feher, F. J. *Langmuir* **1997**, *13*, 4788.
(38) Han, S. W.; Lee, S. J.; Kim, K. *Langmuir* **2001**, *17*, 6981.
(39) Han, S. W.; Kim, K. *J. Colloid Interface Sci.* **2001**, *240*, 492.
(40) de Boer, B.; Meng, H.; Perepichka, D. F.; Zheng, J.; Frank, M. M.; Chabal, Y. J.; Bao, Z. *Langmuir* **2003**, *19*, 4272.
(41) Bandyopadhyay, K.; Vijayamohanan, K. *Langmuir* **1998**, *14*, 625.

(42) Huang, F. K.; Horton, R. C., Jr.; Myles, D. C.; Myles, D. C.; Garrell, R. L. *Langmuir* **1998**, *14*, 4802.
(43) Bandyopadhyay, K.; Vijayamohanan, K.; Venkataramanan, M.; Pradeep, T. *Langmuir* **1999**, *15*, 5314.
(44) Sato, Y.; Mizutani, F. *Phys. Chem. Chem. Phys.* **2004**, *6*, 1328.
(45) Gould, E. S.; McCullough, J. D. *J. Am. Chem. Soc.* **1951**, *73*, 1105.
(46) Köhn, F. Diploma Thesis, Universität Heidelberg, Heidelberg, Germany, 1998.
(47) Heister, K.; Zharnikov, M.; Grunze, M.; Johansson, L. S. O. *J. Phys. Chem. B* **2001**, *105*, 4058.
(48) Shaporenko, A.; Heister, K.; Ulman, A.; Grunze, M.; Zharnikov, M. *J. Phys. Chem. B* **2005**, *109*, 4096.
(49) Wirde, M.; Gelius, U.; Dunbar, T.; Allara, D. L. *Nucl. Instrum. Methods Phys. Res., Sect. B* **1997**, *131*, 245.
(50) Jäger, B.; Schürmann, H.; Müller, H. U.; Himmel, H.-J.; Neumann, M.; Grunze, M.; Wöll, Ch. *Z. Phys. Chem.* **1997**, *202*, 263.
(51) Heister, K.; Zharnikov, M.; Grunze, M.; Johansson, L. S. O.; Ulman, A. *Langmuir* **2001**, *17*, 8.
(52) *Surface chemical analysis-X-ray photoelectron spectrometers-Calibration of the energy scales*; ISO 15472; 2001.
(53) Moulder, J. F.; Stickle, W. E.; Sobol, P. E.; Bomben, K. D. *Handbook of X-ray Photoelectron Spectroscopy*; Chastian, J., Ed.; Perkin-Elmer Corp.: Eden Prairie, MN, 1992.
(54) Frey, S.; Heister, K.; Zharnikov, M.; Grunze, M., Tamada, K.; Colorado, R., Jr.; Graupe, M.; Shmakova, O. E.; Lee, T. R. *Isr. J. Chem.* **2000**, *40*, 81.
(55) Zharnikov, M.; Frey, S.; Heister, K.; Grunze, M. *Langmuir* **2000**, *16*, 2697−2705.
(56) Batson, P. E. *Phys. Rev. B* **1993**, *48*, 2608.
(57) Yang, Y.-W.; Fan, L.-J. *Langmuir* **2002**, *18*, 1157.
(58) Culbertson, R. J.; Feldman, L. C.; Silverman, P. J.; Boehm, H. *Phys. Rev. Lett.* **1981**, *47*, 657.
(59) Citrin, P. H.; Wertheim, G. K.; Baer, Y. *Phys. Rev. B* **1983**, *27*, 3160.
(60) Hsieh, T. C.; Shapiro, A. P.; Chiang, T.-C. *Phys. Rev. B* **1985**, *31*, 2541.
(61) Heister, K.; Rong, H.-T.; Buck, M.; Zharnikov, M.; Grunze, M.; Johansson, L. S. O. *J. Phys. Chem. B* **2001**, *105*, 6888.
(62) Lamont, C. L. A.; Wilkes, J. *Langmuir* **1999**, *15*, 2037.
(63) Varsanyi, G. *Assignments for Vibrational Spectra of Seven Hundred Benzene Derivatives*; Adam Hilger: London, 1974.
(64) Roeges, N. P. G. *A Guide to the Complete Interpretation of Infrared Spectra of Organic Structures*; Wiley: Chichester, U.K., 1994.
(65) Rong, H. T.; Frey, S.; Yang, Y. J.; Zharnikov, M.; Buck, M.; Wühn, M.; Wöll, Ch.; Helmchen, G. *Langmuir* **2001**, *17*, 1582.
(66) Arnold, R.; Azzam, Terfort, A.; Wöll, Ch. *Langmuir* **2002**, *18*, 3980.
(67) Hitchcock, A. P.; Fischer, P.; Gedanken, A.; Robin, M. B. *J. Phys. Chem.* **1987**, *91*, 531.
(68) Stöhr, J. *NEXAFS Spectroscopy*; Springer Series in Surface Science 25; Springer-Verlag: Berlin, 1992.
(69) Azzam, W.; Wehner, B. I.; Fisher, R. A.; Terfort, A.; Wöll, Ch. *Langmuir* **2002**, *18*, 7766.
(70) Zharnikov, M.; Küller, A.; Shaporenko, A.; Schmidt, E.; Eck, W. *Langmuir* **2003**, *19*, 4682.
(71) Chang, S.-C.; Chao, I.; Tao, Y.-T. *J. Am. Chem. Soc.* **1994**, *116*, 6792.
(72) Azzam, W.; Cyganik, P.; Witte, G.; Buck, M.; Wöll, Ch. *Langmuir* **2003**, *19*, 8262.
(73) Cyganik, P.; Buck, M.; Azzam, W.; Wöll, C. *J. Phys. Chem. B* **2004**, *108*, 4989.
(74) Li, Y. G.; DePristo, A. E. *Surf. Sci.* **1996**, *351*, 189.
(75) Cyganik, P.; Buck, M.; Wilton-Ely, J. D. E. T.; Wöll, Ch. *J. Phys. Chem. B* **2005**, *109*, 10902.
(76) Edinger, K.; Gölzhäuser, A.; Demota, K.; Wöll, C.; Grunze, M. *Langmuir* **1993**, *9*, 4.
(77) Poirier, G. E.; Tarlov, M. J. *Langmuir* **1994**, *10*, 2853.
(78) Poirier, G. E.; Tarlov, M. J. *J. Phys. Chem.* **1995**, *99*, 10966.
(79) Poirier, G. E. *Chem. Rev.* **1997**, *97*, 1117.
(80) Poirier, G. E. *Langmuir* **1997**, *13*, 2019.
(81) Cavallini, M.; Aloisi, G.; Guidelli, R. *Langmuir* **1999**, *15*, 2993.
(82) Shaporenko, A.; Brunnbauer, M.; Terfort, A.; Grunze, M.; Zharnikov, M. *J. Phys. Chem. B* **2004**, *108*, 14462.
(83) Zharnikov, M.; Frey, S.; Rong, H.; Yang, Y. J.; Heister, K.; Buck, M.; Grunze, M. *Phys. Chem. Chem.* Phys. **2000**, *2*, 3359.
(84) Azzam, W.; Fuxen, C.; Birkner, A.; Rong, H.-T.; Buck, M.; Wöll, Ch. *Langmuir* **2003**, *19*, 4958.
(85) Heinz, R.; Rabe, J. P. *Langmuir* **1995**, *11*, 506.
(86) Dhirani, A.; Hines, M. A.; Fisher, A. J.; Ismail, O.; GuyotSionnest, P. *Langmuir* **1995**, *11*, 2609.
(87) Charbonneau, G.-P.; Delugeard, Y. *Acta Crystallogr.* **1976**, *B32*, 1420.
(88) Wold, D. J.; Haag, R.; Rampi, M. A.; Frisbie, C. D. *J. Phys. Chem. B* **2002**, *106*, 2813.
(89) Beebe, J. M.; Engelkes, V. B.; Miller, L. L.; Frisbie, C. D. *J. Am. Chem. Soc.* **2002**, 11268.
(90) Yaliraki, S. N.; Kemp, M.; Ratner, M. A. *J. Am. Chem. Soc.* **1999**, *121*, 3428.
(91) Patrone, L.; Palacin, S.; Charlier, J.; Armand, F.; Bourgoin, J. P.; Tang, H.; Gauthier, S. *Phys. Rev. Lett.* **2003**, *91*, 096802/1.